Design and Characterization of a 3D Printed Soft Pneumatic Actuator

Ditzia S. Garcia M.[1], **Serhat Ibrahim**[2], **Benjamin-Hieu Cao**[3] **and Annika Raatz**[4]

Institute of Assembly Technology, Leibniz University Hannover, Garbsen, Germany
[1]*e-mail: garcia@match.uni-hannover.de*
[2]*e-mail: ibrahim@match.uni-hannover.de*
[3]*e-mail: beni.hc@gmx.de*
[4]*e-mail: raatz@match.uni-hannover.de*

Abstract. In soft robotics, the successful development of soft robots involves careful designing that can benefit from current technologies. The use of Finite Element Method (FEM) software and additive manufacturing is essential to optimize the design before fabrication and to facilitate the process. Therefore, we present the design of a 3D printed low-pressure soft pneumatic actuator (SPA) with 3 DoF and a material characterization method to simulate the behaviour of the system. In attempt to define a suitable material modelling method and its reliability to simulate actuator behaviours, we introduce a characterization method and corroborate its efficiency through the evaluation of the performance using the FEM and preliminary tests of the actuator performance. The purpose of this article is to help future projects to effectively simulate the behaviour of 3D printed soft pneumatic actuators to improve the design before fabrication. Throughout the description of the process to effectively fabricate a functional SPA.

Key words: Soft Robotics, Soft Actuators, Modelling, Material Characterization

1 Introduction

Soft robotics is becoming increasingly important due to the paradigm shift from hard to soft materials which aims to improve the human-robot collaboration [1]. By changing the stiffness of the materials used to fabricate robots, more compliant bodies can be achieved. Recent research in the area shows promising results in locomotion, replicating biological organisms that exhibit soft and flexible structures with considerable force [2]. To design systems that can emulate organic mechanisms, the use of uncommon materials and the exploration of new technologies takes a substantial relevance in the research. Currently, soft actuators are mostly fabricated using two methods, casting process and additive manufacturing [3]. On the one hand, casting an actuator requires the use of moulds and multiple fabrication steps to achieve shapes basic geometries like cylinders [4, 5]. Nevertheless, because of the use of moulds, this process has geometrical limitations (e.g. small cavities inside the actuators). Even so, casting permits the use of a wide range of highly stretchable materials [6]. On the other hand, additive manufacturing offers a rapid single instance process achieving similar and even more complex and precise designs [3, 7]. Nonetheless,

in contrast with the casting process additive manufacturing offers reduced material options [8]. Consequently, to explore the use of additive manufacturing optimized designs are required. Smart designs can be achieved through proper optimization. For this, the simulation of the system before fabrication is essential for the user to optimize the design to obtain the required performance. Thus, the correct simulation process has to be achieved through a proper material model suitable for a FEM simulation. For this, we describe the design of a soft pneumatic actuator (SPA) using a 3D printable material. We explain the process for the mathematical model of the material so that a FEM simulation can be set up for the pre-examination of the actuator. The model is validated and evaluated based on data experiments using a commercial angular sensor.

2 DESIGN AND FABRICATION

The actuator described in this article has a general cylinder-like shape (Fig. 1). We used three linear channels separated 120° from each other. Each channel can displace in one direction. They are joined by internal support to provide stiffness to the SPA. Inside this support each channel is connected to a pipe to allow the air injection. For the design of the channels, we chose the concept of PneuNet which originally is formed by an array of chambers connected in series [5]. By using this concept, we guided the deformation areas of the chambers to optimize the pressure (Fig. 1(b)). We modified the geometry of the chambers to adopt a cylindrical shape (Fig. 1(a)). For the dimensions of this actuator, we followed a previous actuator developed by the Institute of Assembly Technologies [4]. The parameters specification of the channels were selected following the results from [9]. We set the chambers wall thickness, the separation between chambers, the internal geometry of the chambers as shown in Fig. 1(a). In this way, a relation of 1:2 between the deformed surface and undeformed surface is used and the chambers deformation focuses on the regions with a smaller wall thickness (Fig. 1(b)).

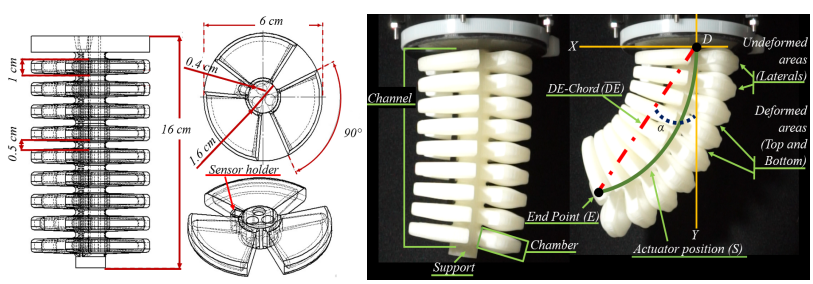

(a) (b)

Fig. 1 3D Printed Soft Pneumatic Actuator. (a) Sketch showing different views of the actuator and its dimensions. (b) SPA view of the actuator without (left) and with pressure(right).

It is important to mention that by changing the amount of chambers and the separation between chambers and channels length we can increase or decrease the angle of deflection [9]. The SPA uses pressure as the actuation method, in this way, the motion starts when the chambers are pressurized with air. During this time the chambers increase the volume and come into contact with each other. This event forces the actuator to bend in the opposite direction (Fig. 1(b)). By pressurizing single or multiple channels, the actuator can displace on different planes (XY and YZ). For the fabrication of the actuator, we use the 3D printer Keyence Agilista and the lowest stiffness silicone AR-G1L available for this printer.

3 Modelling

In soft robotics, the development of reliable models to predict their behaviour increases the potential of successful performance. Although, it is difficult to describe an analytical model of the system due to the non-linearities of the materials and the highly non-linear bending to pressure ratio created by the geometry of the chamber design. An accurate simulation of the behaviour leads to prior optimizations or adjustments of the design before fabrication, saving time and resources [10]. For this reason, we use FEM models (Abaqus CAE) to predict the performance of the system. We find the properties of the material describing a non-linear mechanical behaviour. Additionally, we included a linear elastic approach to help us to observe the differences of the actuator performance to support the use of a non-linear approach for this material.

3.1 Material Characterization

Initially, we performed a series of uniaxial tensile tests following the norm DIN ISO 527 to define the stress-strain relationship. For these tests, we printed specimen and performed 30 tests. The stress-strain relationship of the silicone AR-G1L is showed in Fig. 2. Here, the mean of the data can be observed together with the maximum and minimum values pointed out by the horizontal lines. The standard deviation of the stress is 0.1553 N/mm^2, which is the deviation presented between the different tests. Next, following [13], where the current models for hyperelastic behaviours are mentioned, we chose Mooney Rivlin among other approaches (Ogden, Arruda-Boyce, etc.) as a feasible approach applicable to large strains ($>$ 60 %) analysis. In order to fulfill a FEM model using this approach, we used the energy equation to describe how the deformation affects the energy state of the deformed body. In the FEM analysis software Abaqus the strain-energy ψ equation to appears as

$$\psi = C_1(I_1 - 3) + C_2(I_2 - 3) + \frac{1}{d_1}(J-1)^2. \tag{1}$$

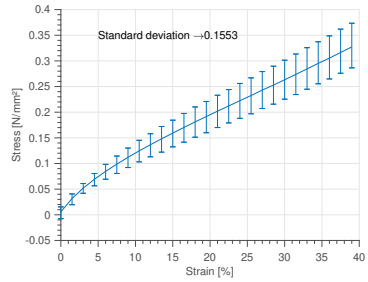

Fig. 2 Stress-strain relationship of the silicone AR-G1L, including the standard deviation of the tensile tests.

In this equation, the material constants for the general deformation are represented by C_1 and C_2 while the constant for volume change of the material is denoted by d_1. These parameters define the behaviour of the material. Additionally, the equation includes the volume-dependent parameter J and the strains in their respective deformation states which are represented by the invariants I_1 and I_2. The parameters I_1 and I_2 are calculated with the right Cauchy-Green tensor $\mathbf{C} \in \mathbb{R}^{3\times3}$ described in [14]. The right Chauchy-Green tensor results from the product of the deformation gradient tensor $\mathbf{F} \in \mathbb{R}^{3\times3}$ and its transposed. The deformation gradient F represents the deformation of a material's point derived from the differential of the spatial directions of the possible displacements. The length variation $\Delta\mathbf{x}$ is the product of the strain ε and x which represents the uni-axial load element of the data for which the stress-strain relation is available with $\mathbf{x} \in \mathbb{R}^{3\times1}$ as the initial coordinate and $\tilde{\mathbf{x}} \in \mathbb{R}^{3\times1}$ as the deformed state of the material point. This function is formulated to analytically model the deformation of the tensile test based on an uniaxially loaded deformation rod. Δx results from the difference of $\tilde{x}$ and x. From this we obtain

$$\frac{\tilde{x}}{x} = (1+\varepsilon). \tag{2}$$

With Eq. (2) we assume that $\lambda = (1+\varepsilon)$. The invariants I_1, I_2 and the volume-dependent J are associated with the strain in deformation gradient F, where in this case, only the first element of the tensor $\mathbf{F}_{11} = \lambda$ is defined by the uni-axial strain state. Assuming that the material is incompressible, the determinant of $\mathbf{F}$ is equal to 1. The determinant of $\mathbf{F}$ results from the multiplication of the diagonal entries, so the two remaining diagonal entries are equal to $\frac{1}{\sqrt{\lambda}}$. This results in the following matrix for the deformation gradient

$$\mathbf{F} = \begin{pmatrix} \lambda & 0 & 0 \\ 0 & \frac{1}{\sqrt{\lambda}} & 0 \\ 0 & 0 & \frac{1}{\sqrt{\lambda}} \end{pmatrix}. \tag{3}$$

Assuming an incompressible material, the parameter approaches the number 0. This leads to a very large number in Eq. (1), but this is compensated by the parameter J.

Since J is the determinant of the deformation gradient due to the incompressibility of the material. With J=1 the last part of the Eq. (1) becomes to 0. The missing parameters C_1 and C_2 in Eq. (1) are determined by an identification procedure. In this case, the model and experimental values of the true stress tensor $\sigma \in \mathbb{R}^{3\times 3}$ are used. To obtain the true stress and the deformation from the Mooney-Rivlin model, we derived the strain-energy with respect to $\mathbf{C}$ to define the second Piola-Kirchhoff stress, where $\tilde{\mathbf{T}}$ is a quantity that describes the stress in a body in an undeformed state [14]. Even though $\tilde{\mathbf{T}}$ does not exist physically, we can use it to calculate the true stress with

$$\tilde{\sigma} = \frac{1}{J}\mathbf{F}\tilde{\mathbf{T}}\mathbf{F}^{\mathsf{T}}. \tag{4}$$

With the stress tensor $\tilde{\sigma}$ calculated from the analytical model, the first element $\tilde{\sigma}_{11}$ was used to calculate the two material parameters C_1 and C_2 using the least square method. This method is implemented in Matlab using the Matlab Optimization Toolbox with the Interior Point method [15] to fit the experimental data series to yield the material parameters. In the step of the calculation of $\tilde{\sigma}$, we use the program Mathematica modified with the package AceGen to generate a Matlab function that derives the stress output for a strain input according to the previously described approach. As a result of this process we obtained $C_1 = 0.1100$, $C_2 = 0.010$ and setted d_1 as 0. After this, we can use the material parameters in Abaqus to describe the behaviour of the material under deformation.

For the linear approach, we used the results from the tensile test (Fig. 2) and linearized the results to find an elastic modulus following the literature [11]. As a result, we find an elastic modulus of 3.1 MPa. Additionally, for a linear approach, a Poisson's Ratio is required. Because we assume our material to be incompressible we find in the same literature the value of 0.5 for incompressible rubber [12].

3.2 Setup simulation

Concerning the configuration of the simulation parameters, we discretized the actuator model in a tetrahedron hybrid element mesh with ten nodes. As a boundary condition, the top end of the SPA is fixed. The load is applied in all inner surfaces of the chambers and tunnels, and is increased up over twelve timesteps from 0 kPa to 12 kPa with an additional gravity step. Additionally, to simulate the forces which appear after the outer chamber surfaces contact, the entire outer surface of the model has an interaction property of tangential behaviour assigned. As a result, we obtained a matrix with the coordinates that describe the displacements of the actuator, which are compared to the movements of the real SPA.

4 Preliminary test

After the simulation, we experimentally corroborated the results of the FEM analysis. For this, we performed displacement tests applying pressure on one chamber at the time. The actuator was displaced to different angular positions, shifting the values between 0° and 40°. During the experiments, we tracked the position using a two-axis bendable sensor. The sensor was positioned on the surface of the support opposite of the activated-channel between two channels (Fig. 1(a)). The test stand for testing the actuators was set up in preliminary work [17]. The acquired data was used to calculate the actuator position (S), which is defined as the central line of the internal support (green curve in Fig. 1(b)). In this way, the sensor angle (α) was used assuming a constant curvature of the actuator [18] to calculate the chord length of the actuator curvature ($\overline{\mathrm{DE}} = \frac{S\sin(\alpha)}{\alpha}$), where S is equal to 13.5 cm. With this, we calculate the position of the point E for any angular value. It is also important to mention that we used only the information which describes a positive displacement meaning that we used the data when the actuator inflates and not when the actuator deflates, due to the inconsistency of the measurements. This is because the recovery time of the material will affect the sensor measurement. With the relevant data, we obtained the angle-pressure relationship of the SPA.

5 Performance evaluation

From the simulation and the experiments, we obtained the position of the actuator in x and y coordinates at 12 kPa since this is the pressure value when the actuator achieves its maximum displacement. The results are presented in Fig. 3(a), here the position of the actuator using the angle sensor, a non-linear model and a linear approach are displayed. In the experiments, we measured an angle of 36.2° at 12 kPa with a constant curvature as the position of the actuator (green diamonds line).

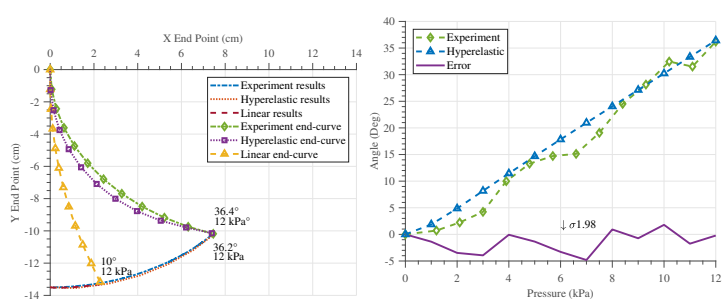

(a) (b)

Fig. 3 Simulation and experiment results. (a) Actuator position S. (b) Angle-Pressure relations of the non-linear simulation and the experiment, and the standard deviation of the results.

While in the simulation with the non-linear model of the actuator, we calculated an angle of 36.4° at 12 kPa with a different curvature (purple squares line) as in the experiments. Regarding the results of the simulation using a linear approach, we calculated an angle of 10° at 12 kPa. Here the position of the actuator at this pressure (yellow triangular line) shows a major displacement from the half of the actuator (from - 6 cm in Y) till the end position of the actuator. From Fig. 3(a), we conclude that the linear approach poorly described the displacement of the actuator in contrast to the experiment results perceiving a difference around 26°. Indicating that the use of a linear approach in this material is not beneficial and does not give accurate information to be used as a reliable source for further simulations. In this way, we can continue with the following results, which are from the non-linear model of the actuator. For this, we decided to compare the relationship between angle and pressure. In Fig. 3(b), we can find the behaviour of the actuator in angular terms while pressure is applied. The simulation results (blue triangular line) showed a smooth displacement of the actuator from 0 to 36.4°, while in the experiments (green diamond line) we can observe abrupt increments at some pressure values. We notice that from the performance of the actuator, the position was affected by the design of the actuator. Because the motion of the actuator starts when the chambers are in contact (section 2), shown in Fig. 1(b). This behaviour was not well appreciated in the simulation results. Thus, as a representative value of this in Fig. 3(b), we showed the error (purple line) between the experiment and the simulation to observe the difference in degrees and its standard deviation to evaluate how much is the difference of the simulation to the experiments.

6 CONCLUSIONS AND FUTURE WORK

In this paper, we presented a 3D printed SPA with its corresponding material characterization and simulation. The SPA simulation was compared with the experiment demonstrating the feasibility of the proposed material characterization method. The presented design reduced the pressure used compared (12 kPa) to similar actuators like in [4] where the working pressure reached 30 kPa, [5] with 74 kPa approximately and [7] with an average working pressure of 60 kPa. This design does not present an increment in length or considerable axial expansion. The simualation approach is close enough to simulate the performance of SPA showing 0.2° at maximum working pressure (12kPa), comparing the results with [5] where the simulation error was greater than 20°. The modelling process presented in this paper can be considered as a plausible approach for soft actuators. In future work, the simulation of the actuator will be extended so that possible fracture points can be predicted. The model developed in this paper will then be used to optimize the design of the 3D printed actuator. In this case, the parameters that are decisive for the deformation, such as chamber distance, number of chambers or wall thickness, will be adjusted using simulation and optimization algorithms to fabricate a more reliable soft actuator which can be used as a manipulator for handling applications.

Acknowledgements This work was supported by the Deutsche Forschungsgemeinschaft (DFG, German Research Foundation) 405030609.

References

1. Polygerinos, P. and Correll, N. and Morin, S. and Mosadegh, B. and Onal, C. and Petersen, K. and Cianchetti, M. and Tolley, M. and Shepherd, R. : Soft Robotics: Review of Fluid-Driven Intrinsically Soft Devices; Manufacturing, Sensing, Control, and Applications in Human-Robot Interaction. Advanced Engineering Materials, **19**, pp. 1438-1656 (2017)
2. Stephen, C. and Carmel, M. and Philip, L. and Jimmy, H. : Bio-inspired soft robotics: Material selection, actuation, and design. Extreme Mechanics Letters, **22**, pp. 51-59 (2018)
3. Schmitt, F. and Piccin, O. and Barbé, L. and Bayle, B. : Soft Robots Manufacturing: A Review. Frontiers in Robotics and AI. **5** (2018)
4. Runge, G. and Peters, J. and Raatz, A. : Design optimization of soft pneumatic actuators using genetic algorithms. In: IEEE Int. Conf. on Robotics and Biomimetics, Macau, pp. 393-400 (2017)
5. Mosadegh, B. and Polygerinos, P. and Keplinger, C. and Wennstedt, Sophia. and Shepherd, R. and Gupta, U. and Shim, J. and Bertoldi, K. and Walsh, C. and Whitesides, G. : Pneumatic Networks for Soft Robotics that Actuate Rapidly. Advanced Functional Materials. **24** (2014)
6. Huichan, Z. and Yan, L. and Ahmed, E. and Robert, S. : Scalable manufacturing of high force wearable soft actuators. Extreme Mechanics Letters, **3**, pp. 89-104 (2015)
7. Kalisky, T. and Wang, Y. and Shih, B. and Drotman, D. and Jadhav, S. and Aronoff-Spencer, E. and Tolley, M. : Differential pressure control of 3D printed soft fluidic actuators. In: IEEE/RSJ International Conference on Intelligent Robots and Systems, Vancouver, pp. 6207-6213 (2017)
8. Zhu, M. and Mori, Y. and Xie, M. and Wada, A. and Kawamura, S. : A 3D printed Two DoF Soft Robotic Finger With Variable Stiffness. 12th France-Japan and 10th Europe-Asia Congress on Mechatronics, 387-391 (2018)
9. Hu, W. and Mutlu, R. and Li, W. and Alici, G. : A Structural Optimisation Method for a Soft Pneumatic Actuator. Robotics, **7**, pp.24 (2018)
10. Moseley, P. & Florez, J. M. & Sonar, H. A. & Agarwal, G. & Curtin, W. & Paik, J. : Modeling, Design, and Development of Soft Pneumatic Actuators with Finite Element Method. Advanced Engineering Materials, **18**, (2015)
11. Peel, L. : P97 Investigation of High and Negative Poisson's Ratio Laminates. International SAMPE Symposium and Exhibition (Proceedings), **50**, (2005)
12. Mott, P. H. and Roland, C. M. : Limits to Poisson's ratio in isotropic materials. Naval Research Laboratory, (2009)
13. Kim, B. and Lee, S. B. and Lee, J. and Cho, S. and Park, H. and Yeom, S. and Han, P. S. : A Comparison Among Neo-Hookean Model, Mooney-Rivlin Model, and Ogden Model for Chloroprene Rubber. International Journal of Precision Engineering and Manufacturing, **13**, (2012)
14. Bonet, J. and Wood, R. : Nonlinear Continuum Mechanics for Finite Element Analysis. Cambridge: Cambridge University Press, pp. 99-160 (2008)
15. Ploskas, N. and Samaras, N. : Linear Programming Using MATLAB®, Springer International Publishing, (2017)
16. Runge, G. and Wiese, M. and Raatz, A. : FEM-Based Training of Artificial Neural Networks for Modular Soft Robots, (2017)
17. Ibrahim, S. and Krause, J. C. and Raatz, A. : Linear and Nonlinear Low Level Control of a Soft Pneumatic Actuator. RoboSoft 2019 IEEE-RAS International Conference, (2019)
18. Webster, R. J. and Jones, B. A. : Design and Kinematic Modeling of Constant Curvature Continuum Robots: A Review. The International Journal of Robotics Research, **13**, pp. 1661–1683 (2010)